Int J Fract (2009) 160:151–167
DOI 10.1007/s10704-009-9415-7

ORIGINAL PAPER

Micromechanical modeling of grain boundary resistance to cleavage crack propagation in ferritic steels

Mateusz Stec · Jonas Faleskog

Received: 3 April 2009 / Accepted: 5 October 2009 / Published online: 24 October 2009

Abstract In ferritic steels a propagating cleavage microcrack changes its propagation direction as it advances from grain to grain. This is due to differences in the orientation of the cleavage planes of two neighboring grains. In order to reach a cleavage plane in a new grain, a microcrack must first penetrate the grain boundary. Grain boundaries therefore act as natural barriers in cleavage fracture. The influence of a grain boundary and the associated misorientation in cleavage planes on crack arrest is here examined using a 3D finite element model with axisymmetric periodicity, representing two grains whose cleavage planes are tilted and twisted relative to each other. The temperature dependent mechanical properties of ferrite are modeled using a temperature dependent viscoplastic response. The development of the crack front as the microcrack penetrates through a grain boundary is here presented. The influence of the twist misorientation on the critical grain size, defined as the largest grain size that can arrest a rapidly propagating microcrack, is examined in a temperature range corresponding to the ductile to brittle transition (DBT) region. It is shown that when both tilt and twist misorientation are present, the influence of tilt and twist, respectively, on crack growth resistance can be decoupled.

Keywords Dynamic fracture · Cleavage fracture · Grain boundary resistance · Crack arrest · Elastic viscoplastic material

M. Stec · J. Faleskog (✉)
Department of Solid Mechanics, KTH Engineering Sciences, Royal Institute of Technology, 100 44 Stockholm, Sweden
e-mail: faleskog@kth.se; jonasf@hallf.kth.se

M. Stec
e-mail: mstec@kth.se

1 Introduction

Structural steels contain a number of imperfections and deviations from crystalline perfection that influence the mechanical behavior. When it comes to fracture toughness, some of the irregularities may promote fracture, whereas others may act as natural barriers against fracture and propagation of a crack. In cleavage fracture, cracking of second phase particles such as carbides frequently acts as a nucleation mechanism of microcracks (McMahon and Cohen 1965; Lee et al. 2002). Particle cracking is a sudden event, which seems to be governed by a weakest link mechanism that depends on the particle size and the stress acting in the particle (Wallin and Laukkanen 2006; Faleskog and Stec 2009). When the stress in the particle becomes sufficiently high, the particle breaks and generates a dynamically growing microcrack that impacts the much tougher surrounding material. Kroon and Faleskog (2005, 2008) numerically examine the critical conditions for continued propagation of such a microcrack. If these conditions are not satisfied, the microcrack will be arrested at the particle/matrix interface or at some limited distance

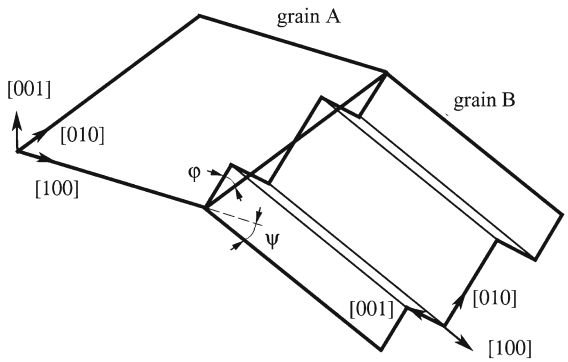

Fig. 1 Characteristic representation of cleavage planes of two neighboring grains and the grain boundary connecting those planes

into the matrix. This process occurs on the sub-micron or micron scale set by the particle size.

The next step in this failure process, i.e. crossing of a grain boundary, is explored by Stec and Faleskog (2009) in a numerical study of the conditions for arrest of a grain sized microcrack at or near a grain boundary. In their work a simplified approach is taken where explicit modelling of the grain boundary is avoided. A grain boundary offers an important resistance to cleavage propagation, since cleavage planes of neighboring grains rarely coincide. This forces an advancing crack front to change its propagation path (McMahon and Cohen 1965; François et al. 1998; Qiao and Argon 2003a,b). Anderson et al. (1994) study growth of a cleavage microcrack by a weakest link mechanism and show that a grain boundary gives contribution to the threshold toughness. Their analysis also show that if a microcrack is to be arrested at a grain boundary, it will most likely occur at the first grain boundary encountered.

Ferritic steels are polycrystals where every grain is surrounded by several others. In such steels with bcc lattice, cleavage fracture mainly occurs along three possible {100} planes (Miller index notation). Since the orientation of the atomic lattice differs between grains, there will be a relative misorientation of the cleavage planes between two neighboring grains. This misorientation can be characterized by a tilt angle ψ and a twist angle φ, as schematically illustrated in Fig. 1. Another important feature at a grain boundary, as indicated in Fig. 1, is that cleavage planes of neighboring grains typically only connect at distinct points. Thus, propagation of a microcrack across a grain boundary must therefore also involve a certain amount of grain boundary sliding/separation before a microcrack fully can penetrate into a consecutive grain (Gell and Smith 1967; Flewitt and Wild 2001).

The most favorable grain orientation for crack propagation is when the normal to a cleavage plane is in the direction of the main loading axis. Cleavage failure then often progress by normal separation along one dominating cleavage plane as is often seen in grains in which a microcrack has nucleated. River patterns in the surrounding grains indicate that cleavage fracture of consecutive grains involves several parallel planes connected by cleavage steps. Qiao and Argon (2003b) and Qiao and Kong (2004) therefore group cleavage planes into primary and secondary planes, primary being those that are more easily separated than secondary and where cleavage of the consecutive grain first takes place. Cleavage failure of these planes are in general of mixed mode type, involving both normal and shear separation that depend on the misorientation angles, especially the twist angle. The twist angle also determines the amount of grain boundary that needs to be separated, if a microcrack is to propagate into a consecutive grain.

Experiments performed by Gell and Smith (1967) and Qiao and Argon (2003a) show that far more resistance to crack propagation results from a twist misorientation (φ) than from a tilt misorientation (ψ). When a microcrack propagates into a new grain, it first penetrates the grain boundary locally at a number of breakthrough points, leaving unbroken grain boundary segments behind. Breakthrough points are located where primary cleavage planes of both grains meet. Failure of the grain boundary segments between the breakthrough points demands a significant amount of work associated with plastic shearing and plastic bending of persistent grain boundary islands, as discussed by Kong and Qiao (2005).

The change in the fracture toughness in the ductile-to-brittle transition (DBT) region is well known. The so called "Master curve" captures this change using only one parameter, the transition temperature (Wallin 1991). Kroon and Faleskog (2005) and Faleskog and Stec (2009) address this change in toughness by studying the effects of plastic rate sensitivity on microcrack nucleation and growth. Their results predict that the critical particle size increases with temperature in the DBT region if plastic rate sensitivity is accounted for. In the companion study by Stec and Faleskog (2009), the influence of plastic rate sensitivity on microcrack

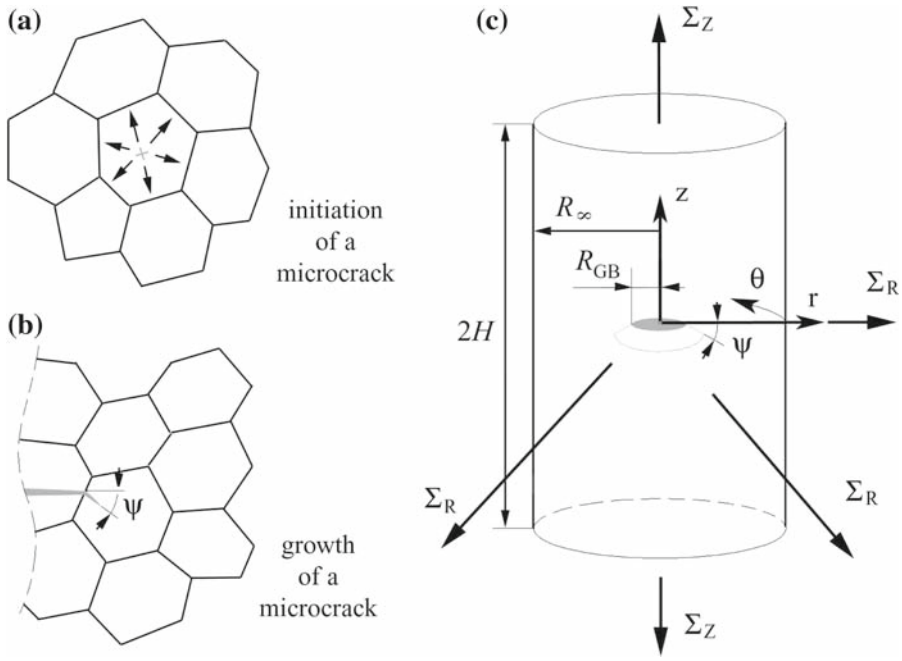

Fig. 2 **a** Initiation and propagation of a microcrack towards a grain boundary (*top view*). **b** Crack path deflection past a grain boundary (*side view*). **c** Idealization of the process (3D model)

propagation across a grain boundary is examined for a misorientation in cleavage planes restricted to a change in the tilt angle, i.e. $\psi \geq 0$ and $\varphi = 0$ (see Fig. 1). In the present work, the micromechanical model developed in Stec and Faleskog (2009) was further improved to incorporate an explicit model of the grain boundary. Thus, the combination of a tilt and twist misorientation between neighboring grains at a grain boundary and how this can act as an obstacle for microcrack propagation will be of special interest here. The role played by plastic rate sensitivity in this failure process will also be examined. The outline of the paper is as follows: the problem and the micromechanical model employed are introduced in Sect. 2. The numerical framework is described in Sect. 3. The general behavior of the model and the results from the numerical analysis are presented in Sect. 4 and then discussed in Sect. 5. Concluding remarks are given in Sect. 6.

2 Problem formulation

2.1 Micromechanical model of cleavage crack growth across a grain boundary

The cleavage fracture scenario to be modelled is summarized as follows: It is assumed that a cleavage microcrack will suddenly form inside a grain at some point in time. The nucleated microcrack will rapidly grow towards the grain boundaries of the surrounding grains, as shown in Fig. 2a. If not arrested inside the grain, the growing microcrack will eventually encounter a grain boundary. Since the orientation of cleavage planes in general differ from grain to grain, the propagation direction will change when a consecutive grain is encountered, see Figs. 1 and 2b. The grain in which the microcrack is initiated will henceforth be referred to as grain A and the consecutive grain as grain B, respectively.

If the cleavage planes of two adjacent grains are twisted relative to each other, these planes only intersect at distinct points (cf. Fig. 1). As a consequence, the portion of the grain boundary linking the cleavage planes between these points becomes involved in the cleavage process. Qiao and Argon (2003b) examine the spacing between intersection points of the primary cleavage planes in a Fe-3Si alloy and find that it does not appear to depend on the twist angle φ. Moreover, they find that the spacing reasonably well follows a log-normal distribution function with a peak value of the distribution of roughly 2.5–3.0 μm, which can be seen as a periodic distance. This experimentally observed regularity was adopted in the present work to develop a periodic micromechanical model.

The topology of the cleavage planes at the grain boundary illustrated in Fig. 1 was modified somewhat in order to make the micromechanical model more adapted for numerical modelling with the finite element method. The stair-way shaped cross section of the cleavage planes of grain B at the intersection of the grain boundary was altered to an isosceles trapezoidal shape. From a numerical point of view, such a change promotes significantly less distorted elements for low twist angles. It also avoids triangular cross sections at the grain boundary and allows for hexahedral meshing of the complex region between the cleavage plane of grain A and the primary and secondary cleavage planes of grain B. The modification is illustrated in Fig. 3a, where the more correct physical topology is depicted by a solid line and the modified shape by a dashed line. In Fig. 3a, φ is the lattice twist misorientation angle introduced in Fig. 1 and w represents the periodic distance between intersection points of the primary cleavage planes of grain A and B. The periodic portion of the grain boundary to be analyzed is thus defined by w. This modification implies that the primary cleavage planes of grain B and the single cleavage plane of grain A meet the grain boundary as parallel lines a distance h apart, and thus never intersect each other. The normal direction of the secondary cleavage planes of grain B will then form an angle $90^\circ - \varphi$ with the normal direction of the primary cleavage planes of grain B (instead of 90°). The height of the trapezoid, $2h$, was chosen such that the total grain boundary surface that must fail during crack advance remained unchanged, i.e. $h/w = (1 - \sqrt{\cos 2\varphi})/(4 \tan \varphi)$, whereas $h_0/w = (\sin 2\varphi)/4$. The ratios h/w and h_0/w are plotted versus the twist angle φ in Fig. 3b. Finally, the grain boundary is considered to be a high angle grain boundary, which is oriented perpendicular to the single cleavage plane of grain A.

The cleavage scenario described was addressed by use of a periodic axisymmetric 3D micromechanical model representing the two grains and the grain boundary. At a certain load level, defined by the true (Cauchy) axial stress Σ_Z and the true radial stress Σ_R, a penny shaped microcrack was initiated centrally in a cylinder with the overall dimensions $2H$ and R_∞, see Fig. 2c, where also the cylindrical coordinate system (r, θ, z) used is defined. The microcrack will then run radially along the single cleavage plane of grain A, coinciding with the plane $z = 0$, until it encounters the grain boundary at $r = R_{GB}$. In grain B, the orientation of the cleavage planes changes according to angles ψ and φ and the microcrack must therefore change its propagation direction in order to advance into the consecutive grain and continue to cleave the structure, which may lead to final failure.

Due to the periodicity of the micromechanical model, only a slice of the geometry presented in Fig. 2c was considered. This slice was defined by $0 \le r \le R_\infty$, $-\Delta\theta/2 \le \theta \le \Delta\theta/2$, $-H \le z \le H$. The angular dimension $\Delta\theta$ is the angular spacing between two points where the cleavage plane of grain A and the primary cleavage planes of grain B meet, hence $w = R_{GB}\Delta\theta$. The slice modeled is delineated by the segment w in Fig. 3a. Boundary conditions corresponding to periodic axial symmetry were applied according to

$$\begin{aligned} &u_r(0, \theta, z) = 0, \\ &u_r(R_\infty, \theta, z) = \bar{u}_r\,(\Sigma_R, \Sigma_Z), \\ &u_r\,(r, -\Delta\theta/2, z) = u_r\,(r, \Delta\theta/2, z), \\ &u_\theta(r, \pm\Delta\theta/2, z) = 0, \\ &u_z\,(r, -\Delta\theta/2, z) = u_z\,(r, \Delta\theta/2, z), \\ &u_z(r, \theta, \pm H) = \pm\bar{u}_z\,(\Sigma_R, \Sigma_Z), \end{aligned} \tag{1}$$

where u_i are components of the displacement vector and $\bar{u}_i$ are components of the displacement vector applied on the remote boundary. A comment is

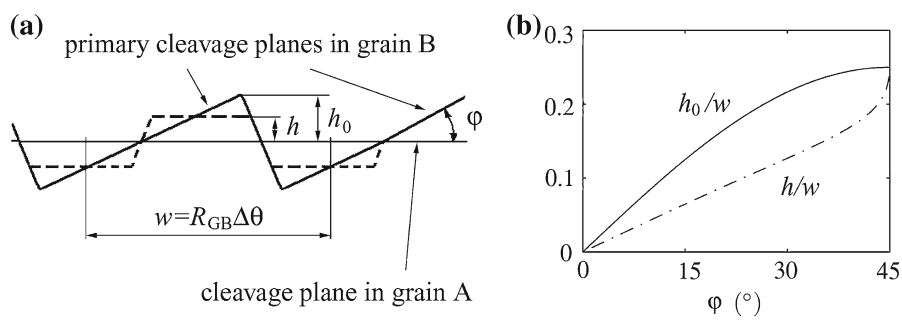

Fig. 3 **a** Modification of the shape of the grain boundary surface and of the cleavage planes of grain B. The *solid line* represents the initial shape, the *dashed line* the modified shape. (**b**) Height of the grain boundary as a function of the twist angle

here in place. It may seem unwise to not utilize the symmetry around $\theta = 0$ of the periodic sector in the numerical analysis, which would allow for modeling of one half-sector. However, the experience gained by the authors in Stec and Faleskog (2009) show that it is necessary to enforce the periodic boundary conditions: $u_r\,(r, -\Delta\theta/2, z) = u_r\,(r, \Delta\theta/2, z)$ and $u_z\,(r, -\Delta\theta/2, z) = u_z\,(r, \Delta\theta/2, z)$, since otherwise a non-symmetric crack growth can take place.

The analysis was performed in two steps. In the initial step the displacements $\bar{u}_i$ were applied quasi-statically in such a way that the stress ratio Σ_R/Σ_Z was kept constant (proportional stressing). We refer to the companion paper (Stec and Faleskog 2009) for details regarding the boundary conditions. The stress ratio is related to the overall stress triaxiality, T, defined as the ratio between mean stress and von Mises effective stress as $T = (1 + 2\Sigma_R/\Sigma_Z)/(3\,|1 - \Sigma_R/\Sigma_Z|)$. In the second step of the analysis, where $\bar{u}_i$ was held constant, the microcrack was nucleated and allowed to run dynamically along the predefined cleavage planes.

The periodic axisymmetric model of the two grains employed here is obviously an idealization. In reality each grain is surrounded by several grains of different sizes, with different lattice orientations. Based on a theoretical model for polycrystals, Smith et al. (2004) predict that three to ten grains surround the cleavage plane of a fractured grain. Qiao and Argon (2003a) examine the fracture surface of a Fe-2%Si alloy and find that a cleaved grain on the average is surrounded by 5.09 neighboring grains. Moreover, Crocker et al. (1996) have identified four different failure mechanisms for grain boundary penetration by cleavage failure. These failure mechanisms are associated with different separation energies (Hamphreys and Hatherly 2004). The crack growth resistance for grain boundary penetration is thus expected to vary depending on which failure mechanism that prevails. Grain B should therefore be seen as an averaged grain that represents all the grains surrounding grain A. In practise, a microcrack may nucleate by cracking of a grain boundary particle. Such a scenario is still covered by the present model provided that the cleavage planes adjacent to the cracked particle do not differ to much. Then, grain A represents all the grains adjacent to the cracked particle.

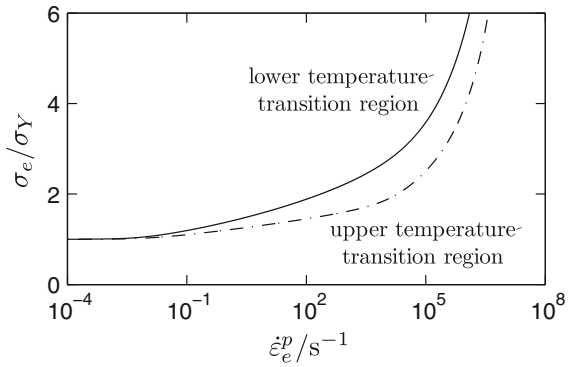

Fig. 4 Viscoplastic law used to represent the rate sensitivity of the ferrite

2.2 Elastic viscoplastic material model

Grains A and B, respectively, were both modeled by an isotropic elastic viscoplastic material. The continuum properties were chosen to be representative of a ferritic steel, with Young's modulus $E = 200\,\mathrm{GPa}$, Poisson's ratio $\nu = 0.3$ and density $\rho = 7800\,\mathrm{kg/m^3}$. The Rayleigh wave speed, approximately given by

$$c_R = (0.862 + 1.14\nu)\,/\sqrt{2\,(1+\nu)^3}\cdot\sqrt{E/\rho} \tag{2}$$

then becomes $c_R = 2908\,\mathrm{m/s}$. The inviscid plastic response was described by the isotropic hardening function

$$\sigma_Y\left(\varepsilon_e^p\right) = \sigma_0\left(1 + \varepsilon_e^p/\varepsilon_0\right)^N, \tag{3}$$

where $\varepsilon_0 = \sigma_0/E$, σ_0 is the initial yield stress, ε_e^p is the equivalent plastic strain and N is the hardening exponent. Both the yield stress and the hardening exponent vary slightly with the temperature in the DBT region, but were set to the constant values $\sigma_0 = 400\,\mathrm{MPa}$ and $N = 0.1$. The value of initial yield stress is higher than the typical value for pure ferrite, but in the range of ferritic steels ($200 - 900\,\mathrm{MPa}$).

The viscoplastic response of the material was described by an overstress model, where the effective stress, σ_e, at plastic loading is defined by

$$\sigma_e = R\left(\dot{\varepsilon}_e^p\right)\cdot\sigma_Y\left(\varepsilon_e^p\right). \tag{4}$$

Here, R is an overstress factor, which is related to the rate of the plastic strain $\dot{\varepsilon}_e^p$, according to

$$\dot{\varepsilon}_e^p = \frac{\dot{\varepsilon}_1 \cdot \dot{\varepsilon}_2}{\dot{\varepsilon}_1 + \dot{\varepsilon}_2}, \qquad \dot{\varepsilon}_1 = \dot{\varepsilon}_0 \left(R^m - 1\right), \\ \dot{\varepsilon}_2 = \dot{\varepsilon}_m \exp\left(-\frac{b}{R}\right), \tag{5}$$

where, $\dot{\varepsilon}_0$, $\dot{\varepsilon}_m$, b and m are material constants. A von Mises type of viscoplastic flow law was used, i.e. the plastic strain increments were defined as $\dot{\varepsilon}_{ij}^p = \dot{\varepsilon}_e^p \, 3s_{ij}/(2\sigma_e)$, where $s_{ij} = \sigma_{ij} - \sigma_{kk}\delta_{ij}/3$. By examination of Eq. (5), it can be seen that the continuum model incorporates a transition in rate sensitivity in agreement with experimental observations on bcc metals (cf. Campbell and Ferguson 1970; Klopp et al. 1985; Tanguy et al. 2000), where the functions $\dot{\varepsilon}_1$ and $\dot{\varepsilon}_2$ represent the rate sensitivity at low and high strain rates, respectively. Two different sets of viscoplastic parameters that represent the temperature range in the DBT region were used:

$$\dot{\varepsilon}_0 = 0.01\,\mathrm{s}^{-1}, \quad m = 15, \quad \dot{\varepsilon}_m = 5 \cdot 10^7\,\mathrm{s}^{-1}, \\ b = 22.09 \\ \dot{\varepsilon}_0 = 0.01\,\mathrm{s}^{-1}, \quad m = 25, \quad \dot{\varepsilon}_m = 5 \cdot 10^7\,\mathrm{s}^{-1}, \\ b = 15.57 \tag{6}$$

The parameters for $m = 15$ and $m = 25$ are here viewed to represent plastic rate sensitivity in the lower and upper ends of the DBT region, respectively. A graphical illustration of the two viscoplastic sets is shown in Fig. 4. The transition in the rate sensitivity for the parameter sets chosen will occur at $\dot{\varepsilon} \approx 5 \cdot 10^3\,\mathrm{s}^{-1}$.

An alternative would be to model the grains by use of crystal plasticity. However, grain B is here assumed to have the average properties of all grains surrounding grain A, and can therefore be considered to mimic a polycrystalline material for which von Mises plasticity is an appropriate model.

2.3 Cohesive surfaces for cleavage crack propagation and grain boundary separation

Dynamic crack growth was modelled by use of cohesive surfaces based on a cohesive law proposed by Kroon and Faleskog (2005), where the effective true (Cauchy) traction t is related to the effective displacement δ ("opening displacement" over the cohesive surface) as

$$t = \sigma_s \cdot \frac{\bar{\delta}}{\left(1 + \bar{\delta}^p\right)^{1/p}} \exp\left(-H\left(\bar{\delta} - 1\right) \cdot \left(\kappa\left(\bar{\delta} - 1\right)\right)^q\right), \\ \bar{\delta} = \delta/\delta_s. \tag{7}$$

Here, σ_s, δ_s, κ, p and q are material constants controlling the surface energy and the shape of the cohesive law and H is the Heaviside step function. This relation is valid as long as the effective displacement is equal to the largest effective displacement experienced. Otherwise the relation is linear and defined as $t = t(\delta_{\max}) \cdot \delta/\delta_{\max}$, where $\delta_{\max}$ is the maximum displacement achieved. The effective traction and displacement are given by

$$\delta = \sqrt{\beta^2\delta_w^2 + \delta_n^2}, \\ t = \sqrt{(t_w/\beta)^2 + t_n^2}, \tag{8}$$

where δ_n and δ_w are the normal and the shear displacements between the separating cohesive surfaces, and t_n and t_w are the corresponding tractions. The mode mixity factor, β, governs the influence of shearing in the cohesive surface. $\beta = 0$ corresponds to a shear stiffness equal to zero and $\beta = 1$ gives the same response in shear as in normal loading.

The area under the curve defined by Eq. (7) represents the work of separation, Γ. The strength of the cohesive zone is denoted $\sigma_{\max}$ and the associated displacement is denoted δ_c. In general $\sigma_{\max}$ is a few percent lower than σ_s and δ_c is always larger than δ_s. In expression (7), t approach zero asymptotically as $\delta \longrightarrow \infty$. In order to give a consistent description of the crack extension, the crack front was taken at the position defined by $\delta = \delta_{tip}$, where δ_{tip} ($> \delta_c$) corresponds to $t = 0.05 \cdot \sigma_{\max}$. For a more extensive outline of the cohesive surface formulation, see Ortiz and Pandolfi (1999) and Roychowdhury et al. (2002). In order to distinguish the parameters of the different grains and the grain boundary the superscripts "A", "B" and "GB" will be used for grain A, grain B and the grain boundary, respectively.

The work of separation, Γ, in the cohesive surface is here viewed as an effective surface energy, which includes energy to break atomic bonds and also some irreversible work dissipated by the advancing microcrack. A value in the range 22 N / m to 34 N / m is considered to give a good fit to experimental results (Curry and Knott 1978), but the slightly larger value 40 N / m was taken for Γ^A. Polycrystals offer greater resistance to fracture than single crystals. This is since multiple cleavage planes and grain boundaries must be broken when a crack front propagates there. Qiao and Argon (2003a) examine the fracture field in a Fe-3%Si alloy and find that the fracture resistance of polycrystals is more than 3 times larger then for single crystals.

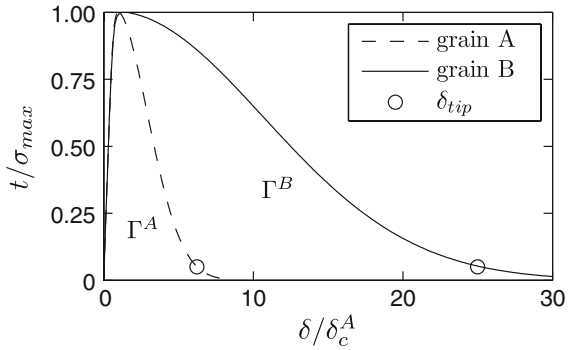

Fig. 5 Traction separation relation used to represent the material separation in grain A and grain B ($\Gamma^B/\Gamma^A = 4$)

Recall that grain B is assumed to represent the average of all the grains surrounding grain A where microcrack nucleation occurs. Therefore, the behavior of a polycrystal was prescribed to grain B, while grain A was given the behavior of a single crystal since it is assumed that cleavage initiates there along a plane perpendicular to the main loading direction. Thus the ratio Γ^B/Γ^A was set to 4 and thereby $\Gamma^B = 160$ N / m. Similar values are also reported from experimental studies by Hahn (1984); Martín-Meizoso et al. (1994) and Linaza et al. (1997) for cleavage crack growth across a ferrite grain boundary.

The ideal strength of ferrite is 12 GPa (Clatterbuck et al. 2003). Due to material defects and dissipative processes it is anticipated that a ferritic material will fail at a lower level and a cohesive strength of $\sigma_{\max} = 4.8$ GPa was therefore used for both grains. The mode mixity was described using $\beta^A = \beta^B = 0.3$ (unless otherwise stated, the influence of these parameters is examined in Stec and Faleskog (2009)). The cohesive laws representing grain A and grain B can be seen in Fig. 5 and the parameters controlling its shape in Table 1.

When a microcrack propagates through a grain boundary it first enters an adjacent grain at breakthrough points, where the primary cleavage planes of both grains meet, and leaves a part of the grain boundary unbroken. The failure of the grain boundary takes place mostly through plastic shear deformation even at temperatures below the DBT temperature (Qiao and Argon 2003a,b). Qiao and Kong (2004) estimate the effective work of separation of the grain boundary to 25 kJ / m. This value includes both the formation of new crack surfaces at the grain boundary and the associated plastic dissipation. Such a high value is explained by development of severe plastic deformation around the grain boundary. In this work, material separation is governed by cohesive models, where the work of separation does not account for plastic deformation in the surrounding material. The effective work estimated by Qiao and Kong (2004) should therefore be seen as an upper limit for the work required to separate a grain boundary and the much lower value $\Gamma^{GB} = 640$ N / m was in general used instead, except in one part of the study where the influence of Γ^{GB} was examined as well. There, the values 160 N / m, 320 N / m and 1,600 N / m were also examined for Γ^{GB}. The mode mixity factor, β^{GB}, was in most cases set to 0.3 except in a few cases where its influence was examined. The other parameters of the cohesive law of the grain boundary are listed in Table 1. The parameters of the cohesive law in both grains and of the grain boundary were taken to be temperature independent.

3 Numerical modeling

The overall dimensions of the cylinder in Fig. 2c were set to $H = R_\infty = 50 R_{GB}$, where H and R_∞ are large enough to avoid wave reflections from the boundary. The slice angle was set to the constant value $\Delta\theta$=0.2 rad.

Table 1 Cohesive zone parameters for grain A, grain B and grain boundary (GB)

	Γ(N/m)	σ_s(GPa)	δ_s(nm)	κ	p	q	δ_{tip}(nm)
Grain A	40	4.92	1.69	0.200	6	2	16.3
Grain B	160	4.82	1.65	4.46e-2	6	2	65.9
GB	160	4.82	1.65	4.46e-2	6	2	65.9
GB	320	4.81	1.65	2.19e-2	6	2	132
GB	640	4.80	1.65	1.09e-2	6	2	264
GB	1600	4.80	1.65	4.33e-3	6	2	661

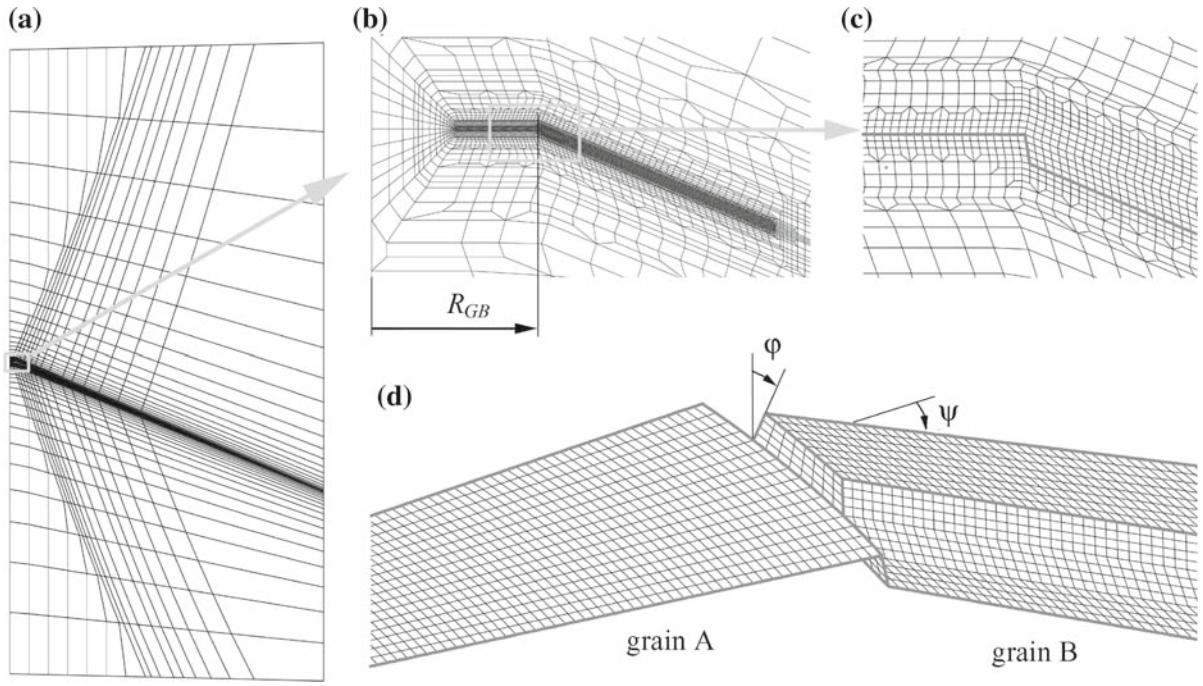

Fig. 6 Finite element mesh representing cleavage planes with misorientation angles $\psi = 22.5°$ and $\varphi = 22.5°$. **a** Side view of a full model. **b** Close up of a fine element layer along the fracture zone. **c** Fine element mesh at the grain boundary. **d** Element mesh of the cleavage planes and the grain boundary (3D visualization)

The analyses were performed using the commercial FEM-program ABAQUS Standard, version 6.6 (2006), employing an incremental-iterative implicit formulation with full Newton iterations to solve the dynamic equilibrium equations. The FEM mesh consisted of between 45,000 and 180,000 3D, 8-node, tri-linear continuum elements and between 4,200 and 17,000 bi-linear cohesive surface elements. The refined mesh region around the cleavage planes, consisted of 16 element layers in the circumferential direction, θ, and extended over the region $0.45R_{GB}$ to $2.5R_{GB}$ in the radial direction, r. In order to correctly resolve the stress field at the crack tip, the characteristic length of the elements adjacent to the cohesive surface was set to 78.4 nm, which is about 30 times δ_c of grain A. A convergence study carried out in the companion study (Stec and Faleskog 2009) showed that this element size provides accurate solutions. An example of an FEM mesh used in the calculations is shown in Fig. 6. In order to obtain sufficiently accurate results, the quasi-static loading phase required about 100 load increments and the subsequent dynamic part of the analysis, between 1,300 and 5,000 steps, depending on the material parameters (viscoplastic and cohesive), misorientation angles (ψ and φ) at the grain boundary and the applied load.

In the dynamic phase of an analysis, the initial growth and velocity of the microcrack was prescribed with a constant velocity equal to $0.4c_R$. This was accomplished by first imposing an effective displacement in the cohesive surfaces equal to δ^A_{tip} on the set of cohesive elements adjacent to $r = 0$, and then in the next set and so on at a rate corresponding to the desired initial crack growth speed. This, procedure was operative until the microcrack was about two elements away from the refined mesh zone shown in Fig. 6b. The number of increments used for surface separation of each set of cohesive elements was large enough to closely follow the traction separation law. At rare occasions, the increment in the effective true traction, t, was about $0.2\sigma_{\max}$ but most of the time it was much smaller. Both the initial velocity and the length of the zone where initial crack propagation is controlled can be set to different values. Variation of these parameters

was investigated by the authors in Stec and Faleskog (2009), and it was there shown that moderate deviations around the values chosen here had minimal effect on the final results.

The key question to be answered in this study was: Given an overall stress state and grain orientation, what is the largest size of grain A, denoted the *critical grain size* R^c_{GB}, that will cause a rapidly propagating microcrack to be arrested. Due to the difference in toughness between grain A and grain B ($\Gamma^B/\Gamma^A = 4$), the microcrack will be arrested if $R_{GB} \leq R^c_{GB}$ or experience sustained propagation if $R_{GB} > R^c_{GB}$. The critical grain size R^c_{GB} was calculated by an iterative procedure, by repeating the analysis until the difference between an upper bound (R^p_{GB}) and a lower bound (R^a_{GB}) for the target value R^c_{GB} satisfied the convergence criterion: $R^p_{GB} - R^a_{GB} < \Delta R_{GB}$, where the tolerance ΔR_{GB} in most cases was set to 0.1 μm. However, as will be seen below, for the final value of R^a_{GB} satisfying the convergence criterion, arrest did not occur at the grain boundary, but at some distance into grain B. A good estimate of the size of the arrested microcrack required a tighter tolerance, and when the arrest length was of interest, a tolerance $\Delta R_{GB} = 0.001$ μm was used. Each time an analysis for a new grain size was performed, a new mesh was generated.

4 Numerical results

In the companion article (Stec and Faleskog 2009), the model parameters are systematically studied for the simplified case of a pure tilt misorientation of the cleavage planes. There, the critical grain size is carefully examined for a remotely applied stress in the interval $3.2\sigma_0 \leq \Sigma_Z \leq 3.8\sigma_0$ with stress ratios (triaxiality) in the range $0.55 \leq \Sigma_R/\Sigma_Z \leq 0.70$. Here, we present results on how crack growth resistance is affected by a combined tilt and twist misorientation. The influence of dissipation associated with grain boundary sliding/separation, and how this is influenced by plastic rate sensitivity in the DBT region, is also investigated. This rather complex cleavage failure process, involving a grain boundary, depends on a number of material parameters that can be expressed in non-dimensional forms and classified as follows:

- Rate independent elastoplasticity: $\sigma_0/E,\ \nu,\ N$
- Rate dependent plasticity: $\dot{\varepsilon}_0\Gamma^B E/\left(c_R\,\sigma_0^2\right),\ m$
- Primary/Secondary cleavage planes: $\psi, \varphi, \Gamma^B/\Gamma^A, \Gamma^B E/\left(R_{GB}\,\sigma_0^2\right), \sigma_{\max}/\sigma_0, \beta^B$
- Grain boundary sliding/separation: $\varphi, \Gamma^{GB}\,w/\left(\Gamma^B\,R_{GB}\right),\ \beta^{GB}$

The numerical computations proved to be very time consuming, and only key parameters associated with the grain boundary could for practical reasons be investigated. Also, only one applied stress state will be considered, since the influence of applied stress state (especially effects of triaxiality) is carefully investigated and discussed in the companion article. To summarize, the critical size of grain A will be evaluated as a function of the selected set of key parameters according to

$$R^c_{GB} = F\left(\psi, \varphi, \frac{\Gamma^{GB}}{\Gamma^B}\Delta\theta, \beta^{GB}; m\right), \tag{9}$$

for a remotely applied stress $\Sigma_Z = 3.6\sigma_0$ with $\Sigma_R/\Sigma_Z = 0.65$. Note that in Eq. (9), the ratio w/R_{GB} is replaced by $\Delta\theta$ (cf. Fig. 3a), which was constant and not changed in the numerical analyses.

4.1 General behavior

The characteristic behavior of a microcrack that grows across a grain boundary within the realm of the present micromechanical model is displayed in Fig. 7 for a case of pure twist misorientation with $\varphi = 22.5°$ ($\psi = 0°$) and plastic rate sensitivity exponent $m = 25$. This Figure shows isocontours of the effective traction on the cohesive surfaces at five different stages during the advance of a microcrack. Fig. 7a–c pertain to grain boundary penetration, Fig. 7d corresponds to crack arrest, and Fig. 7e to a case of continued growth approaching steady state conditions. The general picture from experimental observations is also recognized here, i.e. that when a crack front penetrates a grain boundary, it first grow along the more favorable primary cleavage planes of the neighboring grain and leaves secondary cleavage planes and an unbroken grain boundary behind (Qiao and Argon 2003a; Qiao and Kong 2004; Kong and Qiao 2005).

Initially, the microcrack grows radially along the single cleavage plane of grain A until the grain boundary is encountered, see Fig. 7a. The microcrack then makes a temporary stop until sufficient energy has been released at the crack front in order to overcome the higher work of separation of the new encountered

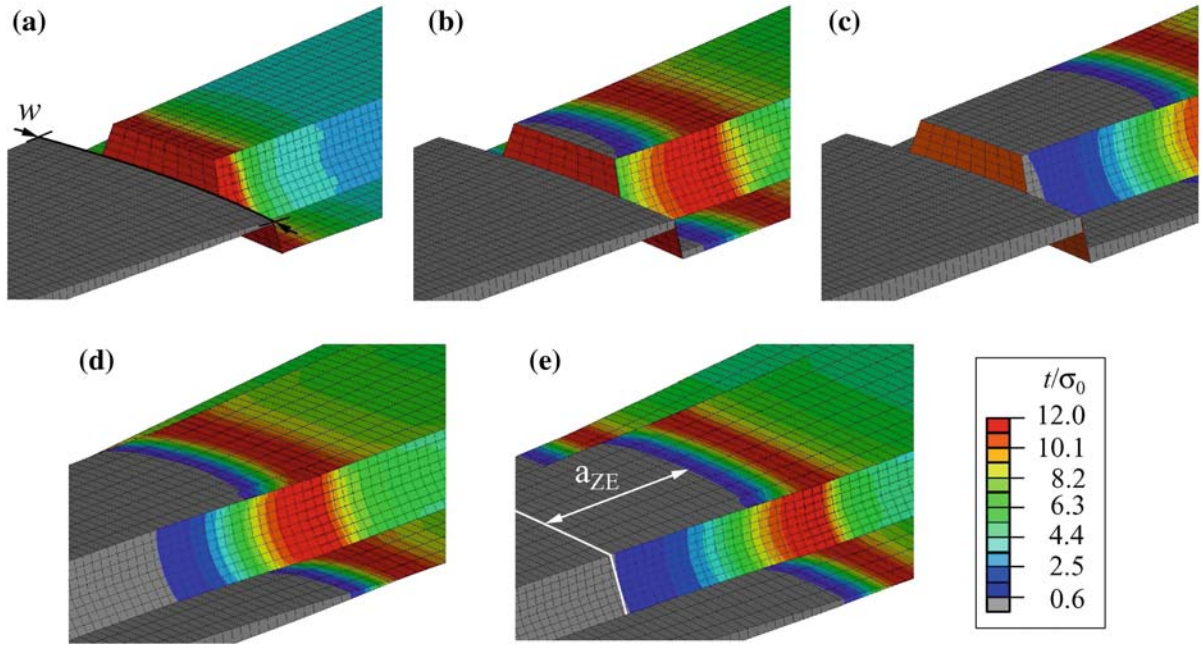

Fig. 7 Crack profiles and isocontours of effective traction on cohesive surfaces. **a** Propagating microcrack at the grain boundary. **b** Insipient breakthrough. **c** Breakthrough. **d** Arrested microcrack. **e** Cleavage. Here, gray color represents new crack surface ($t < 0.05\sigma_{\max}$)

cleavage planes. The primary cleavage planes of grain B are the first ones to fail and a crack front with a shape of a convex circular arc develops. At this incipient breakthrough, the separation of the secondary cleavage planes is small and the advancing crack front is effectively held back, see Fig. 7b. As the separation of the secondary cleavage planes increases, the crack front in the primary cleavage planes advances. At some point, the secondary cleavage planes fail and the whole crack front enters into grain B, see Fig. 7c. This incident defines breakthrough in the present model. At this point, the numerical result shows that the grain boundary surface is still in the process of separation and continues to offer resistance but with an influence that decreases as the crack front continues to propagate away from the grain boundary. The characteristic profile of the crack front at breakthrough, i.e. an advanced front in the primary cleavage planes and with a front in the secondary cleavage planes that lag behind, prevails until the event of crack arrest as shown in Fig. 7d as well as for the case of continued growth as noted in Fig. 7e. The difference between the crack fronts in the primary and secondary cleavage planes depicted as a_{ZE}, in Fig. 7e and here called the *zone of extent*, changes during the propagation history. For the cases presented here, a_{ZE} decreases when approaching crack arrest (compare Fig. 7c with d), and increases as the crack continues towards macro cleavage Fig. 7e.

The peak value of the effective traction in the cohesive surface (associated with δ_c) occurs several elements ahead of the current crack front (defined at $\delta = \delta_{tip}$), as can be observed in Figs. 7a–e. The smooth variation of the effective traction indicates that the traction separation law used, Eq. (7), was correctly resolved in the analysis. Furthermore, by assessing the distance between the trajectory of the peak value and the current crack front, the extent of the active cohesive zone can be estimated to about $0.5w$.

The zone of extent, a_{ZE}, will now be examined more closely. As noted above, a_{ZE} changes during the propagation history. In Fig. 8 the zone of extent is plotted versus the twist misorientation angle, φ, at two different instances: breakthrough and arrest. It can clearly be seen that a_{ZE} decreases with an increasing φ, which is valid for both breakthrough

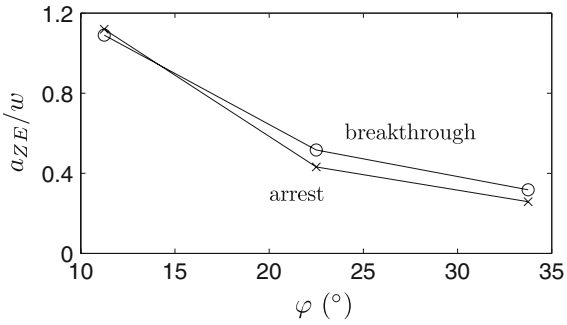

Fig. 8 Size of the zone of extent at breakthrough and arrest

and arrest. This may be explained considering that the area of secondary cleavage planes, which are less favorable for cleavage, increases with an increase in twist misorientation, while the area of the more cleavage apt primary planes decreases. Moreover, the distance between the secondary cleavage planes decreases with an increase in the twist angle, and at the same time the area of secondary cleavage planes increases relative to the area of primary cleavage planes. As a result, the primary cleavage planes become less dominant, which supports the trend noted in Fig. 8.

For a case of continued growth ($a \gg R_{GB}$) an opposite effect on a_{ZE} may be anticipated from Fig. 7e. As the crack progresses into grain B, the area of the secondary cleavage planes remain constant, whereas the relative amount of primary cleavage planes increases in proportion to the radial extent of the microcrack. This, feature of the present model is not viewed as an artifact, as it is also seen in experiments. Thus, the relative influence of secondary cleavage planes will decrease with crack growth to the benefit of the primary cleavage planes, and as an outcome, an increase in a_{ZE} would be expected.

4.2 Grain boundary resistance

When the cleavage planes of two adjacent grains are twisted relative to each other, a microcrack must also to some extent propagate along the grain boundary in order to cleave both grains. Both grain boundary sliding/separation and plastic deformation around the grain boundary take place, which requires extensive work, as discussed by Qiao and Kong (2004).

Figure 9a shows how the grain boundary toughness, Γ^{GB}, and the mode mixity factor, β^{GB} (relating shear strength to cohesive strength as $\tau_{\max} = \beta^{GB}\sigma_{\max}$) affect the critical grain size, R^c_{GB}. Here, a high angle grain boundary is considered, defined by $w/R_{GB} = 0.2$, $\varphi = 22.5°$ and $\psi = 0°$, at a temperature corresponding to $m = 25$. The three different R^c_{GB} versus Γ^{GB}/Γ^B curves in Fig. 9a pertain to β^{GB} equal to 0.3, 0.6 and 1.0, respectively. It is clear that a grain boundary exerts a profound effect on the critical grain size R^c_{GB}. In the absence of a twist misorientation and thus in the absence of an active grain boundary ($\varphi = 0°$), Stec and Faleskog (2009) obtain $R^c_{GB} = 11.91\ \mu$m, whereas in Fig. 9a $R^c_{GB} > 15.5\ \mu$m for all three β^{GB} values considered. From Fig. 9a it can be observed that β^{GB}, and thus the shear strength of the grain boundary, has a strong effect on the critical grain size. The grain boundary toughness also affect the critical grain size somewhat, but this influence is not as strong and does not change much for $\Gamma^{GB}/\Gamma^B > 4$. However, there exists a synergy effect between β^{GB} and Γ^{GB} on R^c_{GB}. If the shear strength of the grain boundary increases (β^{GB} increases), the relative influence of the grain boundary toughness on the critical grain size is enhanced. For instance, over the Γ^{GB}/Γ^B range covered in Fig. 9a, the critical grain size increases by 5% for $\beta^{GB} = 0.3$ and by 22% for $\beta^{GB} = 0.6$. It should be mentioned that R^c_{GB} pertaining to the curve $\beta^{GB} = 1.0$ at $\Gamma^{GB}/\Gamma^B = 2$ was obtained within a tolerance of 0.625 μm (indicated by the vertical tolerance bar), while a tolerance less than 0.1μm was used for the other cases.

The numerical results revealed another interesting effect of the grain boundary shear strength. If the shear strength becomes sufficiently large a microcrack will always be arrested at the grain boundary if the conditions for sustained propagation are not fulfilled. In Fig. 9b, the arrest lengths, a^{arrest}, corresponding to the critical grain sizes at $\Gamma^{GB} = \Gamma^B$ in Fig. 9a are shown as a function of β^{GB}. Note that when $\beta^{GB} = 0.3$, crack arrest occurs inside grain B ($a^{arrest} \approx 1.35 R^c_{GB}$), whereas crack arrest occurs at the grain boundary if $\beta^{GB} = 1.0$. The arrest length is here evaluated as the average of the radial distance to the crack front projected onto the plane $z = 0$. The influence of Γ^{GB}, in the range Γ^B to $10\Gamma^B$, on a^{arrest} was also examined for $\beta^{GB} = 0.3$. These calculations resulted in a^{arrest} values that scattered from $1.27 R^c_{GB}$ to $1.36 R^c_{GB}$, where no systematic trend depending on Γ^{GB} was found. A tolerance of 0.001μm was used in these arrest analyses.

As mentioned in connection with Fig. 7c, failure of a grain boundary does not occur at the instant of

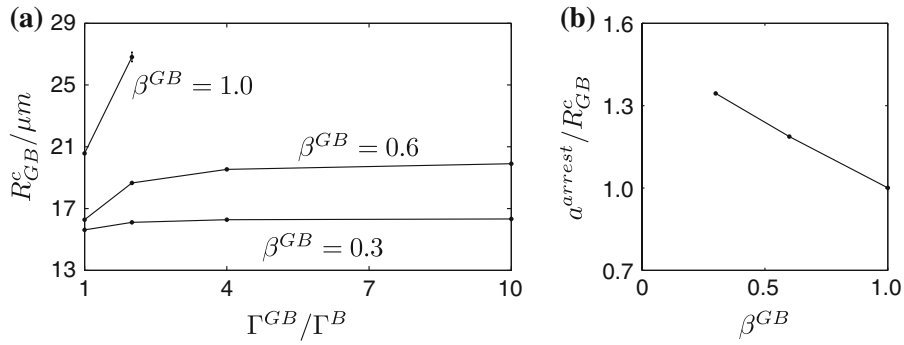

Fig. 9 **a** Influence of the grain boundary toughness and of the shear strength on the critical grain size. **b** Influence of the shear strength on the crack arrest length

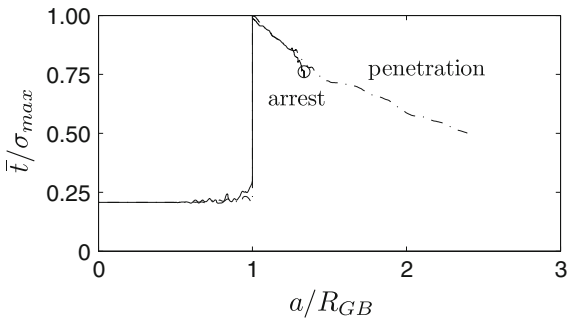

Fig. 10 Grain boundary traction as a function of the microcrack size for cases corresponding to arrest and penetration

breakthrough into an adjacent grain. Thus, the grain boundary continues to contribute to crack growth resistance long after the microcrack has left the grain boundary. This phenomenon is demonstrated in Fig. 10, showing the relation between the grain boundary average value of the effective traction, $\bar{t}$, and the normalized crack length a/R_{GB}. It should be pointed out that the predominate contribution to the effective traction in the cohesive surface elements at the grain boundary is due to shearing (all cohesive elements at the grain boundary have their normal vector initially pointing in the radial direction). Therefor, $\bar{t}$, evaluated as the average value of effective traction (t) over the whole grain boundary surface, should be interpreted as the average shear traction acting on the grain boundary in the direction of the main loading axis (z-axis). The crack length, a, is extracted from the relation, $A = a^2\Delta\theta/2$, where A denotes the area of failed cohesive elements ($\bar{t} < 0.05\sigma_{\max}$) projected on the plane $z = 0$.

In Fig. 10, the results again pertain to $\psi = 0°$, $\varphi = 22.5°$ and $m = 25$. The two curves correspond to microcracks that in one case nucleates in a grain of size $R_{GB} = 16.274\,\mu\text{m}$, which eventually will be arrested, and in the other case nucleates in a grain of size $R_{GB} = 16.275\,\mu\text{m}$, which will experience sustained growth. As discussed above, recall that the effective traction on the grain boundary essentially corresponds to shear traction, i.e. $t_w \gg t_n$ in Eq. (8). When the microcrack advances in grain A, both cases follow the same curve as they should. As the microcrack reaches the grain boundary, $\bar{t}$ rises steeply until the value of the cohesive strength is reached. After breakthrough into grain B, $\bar{t}$ only slowly decays as the crack front advances. For the microcrack that arrests at $a = 1.34R_{GB}$, a residual value of about $0.76\sigma_{\max}$ is recorded for $\bar{t}$. For the case of sustained growth, the value of $\bar{t}$ continues to decrease as the front of the microcrack advances. Thus, the grain boundary then affects the growing microcrack by acting as a line force behind the crack front. However, the resistance to crack propagation offered diminishes, when the crack front moves away. This is since the effective traction, the magnitude of the line force, decreases and the distance between the line force and the crack front increases. The calculations for the penetration case in Fig. 10 was interrupted when a had reached almost $2.5R_{GB}$ and $\bar{t}$ had decreased to about $0.5\sigma_{\max}$, since the numerical model primarily was designed to accurately capture the crack arrest. Thus, the crack must propagate much further in order to obtain complete grain boundary failure ($\bar{t} < 0.05\sigma_{\max}$).

4.3 Influence of twist angle and temperature on arrest

Above it was shown that secondary cleavage planes effectively hold back a propagating microcrack. With an increasing twist angle, the size of the secondary cleavage planes increases and so does the part of the

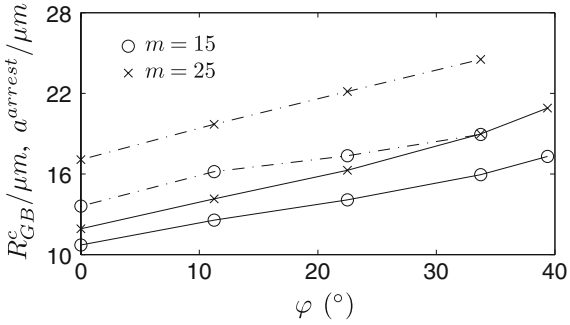

Fig. 11 Influence of the twist angle on the critical grain size (*solid thin line*) and its corresponding crack arrest length (*dashed-dotted line*) at temperatures corresponding to $m = 15$ and $m = 25$. Load case: $\Sigma_Z = 3.6\sigma_0$, $\Sigma_R/\Sigma_Z = 0.65$

grain boundary that must separate before final failure can take place. In Fig. 11 the critical grain size and its corresponding arrest length, a^{arrest}, are presented as a function of the twist misorientation angle, φ, for a grain boundary without tilt misorientation ($\psi = 0°$). Two plastic rate sensitivity exponents are considered $m = 15$ and 25, representing a lower and an upper temperature in the DBT region, respectively. At both temperatures, R^c_{GB} and a^{arrest} increase with an increase in the twist misorientation. The increase in the critical grain size is initially fairly linear but further enhanced at higher twist angles. From Fig. 11 it can be seen that the critical grain size increases by 62% for $m = 15$ and by 75% for $m = 25$, when φ changes from 0° to 39.4°.

For all cases presented in Fig. 11, a running microcrack managed to fully penetrate the grain boundary before it was arrested at some distance into grain B. Even though the arrest length increases with an increasing twist misorientation, the arrest occurs comparatively closer to the grain boundary at a high φ value. For instance, when φ increases from 0° to 33.75°, the ratio a^{arrest}/R^c_{GB} decreases from 1.27 to 1.19 for $m = 15$, and correspondingly from 1.43 to 1.29 for $m = 25$.

The influence of the temperature (by changes in m) is thoroughly investigated in the companion study (Stec and Faleskog 2009). There, for a pure tilt misorientation ($\psi = 22.5°$, $\varphi = 0°$), it is shown that when the temperature is elevated in the DBT region, effectuated by a change in m from 15 to 25, the critical grain size increases by 10% to 18% depending on the applied stress state. In the present study, so far only considering a pure twist misorientation ($\psi = 0°$) with $\Sigma_Z = 3.6\sigma_0$ at $\Sigma_R/\Sigma_Z = 0.65$, the increase in critical grain size in the DBT region is 11% when $\varphi = 0°$ and as much as 21% when $\varphi = 39.4°$, as shown by the result presented in Fig. 11. This clearly indicates that the increase in the critical grain size in the DBT region is not only due to a change in plastic rate sensitivity. There also exists a synergistic effect of a change in plastic rate sensitivity combined with a lattice misorientation at a grain boundary (mismatch in cleavage planes between neighboring grains).

In Fig. 12 the results from the companion study (Stec and Faleskog 2009), pertaining to a pure tilt misorientation ($\varphi = 0°$) are compared with the results shown in Fig. 11 corresponding to a pure twist misorientation

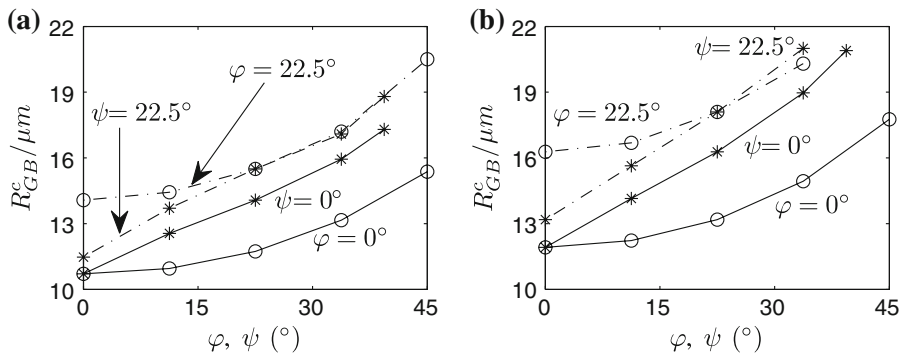

Fig. 12 Influence of the tilt angle (ψ), the twist angle (φ) and the combination of them on the critical grain size. Load level: $\Sigma_Z = 3.6\sigma_0$, $\Sigma_R/\Sigma_Z = 0.65$. **a** Lower transition temperature, $m = 15$. **b** Upper transition temperature, $m = 25$. *Solid lines* represent data where one angle is held zero, *dash-dotted lines* where one angle is 22.5°, *stars symbols* where tilt is held constant and *circle symbols* where twist is held constant

($\psi = 0°$). Fig. 12a shows the relation between R^c_{GB} and the misorientation angles for a temperature in the lower DBT region ($m = 15$) and Fig. 12b for a temperature in the upper DBT region ($m = 25$). The solid line marked by circle symbols depicts a pure variation in the tilt angle ψ with $\varphi = 0°$, and the solid line marked by star symbols depicts a pure variation in the twist angle φ with $\psi = 0°$. The results for both temperatures examined clearly demonstrate that the critical grain size is far more influenced by a change in the twist angle, φ, than for a change in the tilt angle, ψ. It can thus be concluded that a twist misorientation offers more resistance to crack propagation than a tilt misorientation. This is in accordance with experimental observations by Gell and Smith (1967) and by Qiao and Argon (2003a,b).

The effects from a combination of a tilt and twist misorientation are addressed next. The dot-dashed curves in Fig. 12 demonstrate the combined effect of changes in the angles ψ and φ. Here, the dot-dashed curve marked by circle symbols pertains to a variation in the tilt angle ψ for the constant twist angle $\varphi = 22.5°$, and the dot-dashed curve marked by star symbols pertains to a variation in the twist angle φ for the constant tilt angle $\psi = 22.5°$. First, note that the dot-dashed curves coincide at $\psi = \varphi = 22.5°$, as required. From this point, the dot-dashed curves fall close together as the misorientation angle (the one that is permitted to vary) increases from 22.5°. This can be understood from the behavior of the solid curves that exhibit about the same rate of change with an increase in the misorientation angle beyond 22.5°. A difference in R^c_{GB} between the dot-dashed curves is noted below 22.5°. This difference increases as the misorientation angle decreases from 22.5° to 0°, and at 0° it is equal to the difference in R^c_{GB} recorded between the solid curves at 22.5°, as expected. A closer examination of these results reveals that, at a given temperature (given m value), the critical grain size can be phrased as a function of the lattice misorientation angles ψ and φ, where the variables ψ and φ are separated as

$$R^c_{GB}(\psi,\varphi) = R^c_{GB}(0°,0°) \cdot \frac{R^c_{GB}(\psi,0°)}{R^c_{GB}(0°,0°)} \cdot \frac{R^c_{GB}(0°,\varphi)}{R^c_{GB}(0°,0°)}. \quad (10)$$

If compared with the numerical data points in Figs. 12a, b, expression (10) deviates at most by 1.0%, which is valid for all the numerical data points except two, where the difference was less than 2.1%. Thus, by decoupling the dependence of the angles ψ and φ, the critical grain size can for the case investigated be written on the general form

$$R^c_{GB}(\psi,\varphi) = R^c_{GB}(0°,0°) \cdot f(\psi) \cdot g(\varphi). \quad (11)$$

5 Discussion

Grain boundaries in polycrystalline materials are often the last obstacles before a dynamically propagating microcrack can form a macrocrack that leads to final failure of a structure. At a grain boundary, the propagation direction of a microcrack must in general change in order to conform to the cleavage planes of a consecutive grain. If the grain boundary is a low angle grain boundary it offers relatively little resistance to a microcrack before it enters into a neighboring grain (Gell and Smith 1967). However, if a microcrack hits a high angle grain boundary and is not arrested, it starts to penetrate into the adjacent grain at points where the cleavage plane of the initial grain meet the primary cleavage planes of the consecutive grain. This zone of extent then grows, leaving a part of the grain boundary unbroken. At some point, the part of the crack front still being locked at the grain boundary can no longer be held back, and the microcrack fully enters into the consecutive grain, as discussed by Qiao and Argon (2003b). This behavior was well captured by the model developed in the present study, although the topology of the cleavage planes in a consecutive grain were slightly different if compared to the more physically realistic conditions schematically shown in Fig. 1.

Fracture tests carried out in the DBT region strongly suggest the existence of a threshold fracture toughness. Some experiments also suggest that this threshold increases with temperature (cf. Faleskog et al. 2004). It is reasonable to assume that the threshold value must be associated with the micromechanisms governing cleavage fracture, where barriers against microcrack propagation such as a particle/ferrite interface and grain boundaries play a crucial role. The results presented here and in the companion paper (Stec and Faleskog 2009) clearly show that the possibility for a dynamically running microcrack to penetrate a grain boundary becomes significantly more difficult as the temperature increases. Thus, lending numerical support to a threshold value that increases with temperature.

In Sect. 4, the influence of a combination of tilt and twist misorientation angles ψ and φ on the critical grain

size was explored. The numerical results show that the influence of tilt and twist is decoupled such that R^c_{GB} can be written according to Eq. (11). Possible analytical expressions for the angle functions $f(\psi)$ and $g(\varphi)$ in Eq. (11) will now be discussed.

The Griffith criterion relates the axial load to a the critical size of a microcrack as $a_G = (\pi E\Gamma)/\left[4\left(1-\nu^2\right)\Sigma_Z^2\right]$. In particular, this expression pertains to a flat penny shaped crack with radius a_G, and does not account for a possible kink due to a change in the orientation of cleavage planes. Gell and Smith (1967) study the propagation of cracks through grain boundaries and present two expressions for the reinitiation of a flat microcrack subjected to a uniform internal pressure when the cleavage plane of the next grain is either tilted or twisted relative to the initial grain (microcrack). In order to describe the increase in crack growth resistance, those expressions can be reorganized as $a_k/a_0 = \cos^{-4}(\psi/2)$ for a tilt misorientation and $a_k/a_0 = \cos^{-4}(\varphi)$ for a twist misorientation. Here, a_k is the critical crack size for a microcrack that must change its propagation direction and a_0 is the critical crack size for microcrack that continues to run straight. These expressions are decoupled in the same manner as Eq.(11) (cf. Gell and Smith 1967), and will henceforth be referred to as $f_{GS}(\psi) = \cos^{-4}(\psi/2)$ and $g_{GS}(\varphi) = \cos^{-4}(\varphi)$, respectively.

Qiao and Argon (2003b) present an alternative expression for a high angle grain boundary, and propose that the effective toughness of crack growth across a grain boundary, Γ_{eff}, can be related to the toughness of a single crystal, Γ, according to

$$\frac{\Gamma_{eff}}{\Gamma} = \frac{\sin\varphi + \cos\varphi}{\cos^2\psi} + 0.25\frac{\sin\varphi\cos\varphi}{\cos\psi}. \tag{12}$$

Here, the first term is connected to the amount of cleavage planes in the consecutive grain, and the second term is connected to the amount of grain boundary involved in the penetration process. With recourse to the Griffith criterion, where the critical crack size is proportional to the critical energy release rate, the left hand side of Eq. (12) can be replaced by the ratio a_k/a_0 introduced above. As noted, Eq. (12) does not immediately conform to relation (11), where the dependence of ψ and φ is decoupled. However, keeping the structure of Eq. (10) in mind, and by evaluating Eq. (12) for $\varphi = 0$ and $\psi = 0$, the functions $f(\psi)$ and $g(\varphi)$, respectively, in Eq. (11) may be identified as $f_{QA}(\psi) = \cos^{-2}(\psi)$ and $g_{QA}(\varphi) = \sin(\varphi) + \cos(\varphi) + 0.25\sin(\varphi)\cos(\varphi)$.

The expressions $f_{GS}(\psi)$ and $g_{GS}(\varphi)$ proposed by Gell and Smith (1967) (referred to as GS below) and expressions $f_{QA}(\psi)$ and $g_{QA}(\varphi)$ emanating from Qiao and Argon (2003b) (referred to as QA below), can now be inserted into the general decoupled form of the critical grain size, i.e. Eq. (11). To facilitate a comparison with the numerical results from the micromechanical model, the value $R^c_{GB}(0°, 0°)$ is evaluated from a solution with $\Sigma_Z = 3.6\sigma_0$, $\Sigma_R/\Sigma_Z = 0.65$ and $m = 25$. In Fig. 13, predictions of the critical grain size is compared with the micromechanical results. In Fig. 13a the twist angle is set to zero and in Fig. 13b the tilt angle is set to zero, in order to simplify a comparison.

As seen in Fig. 13a, the influence of the tilt angle is significantly overestimated by the QA-prediction, and slightly underestimated by the GS-prediction, if compared to the results from the micromechanical model (circle symbols). However, both predictions are based on cosine functions that give the right trend. In this exploratory study, two similar cosine functions chosen in an ad hoc way as $f_1 = \cos^{-1}(\psi)$ and $f_2(\psi) = \cos^{-5}(\psi/2)$, were examined as well. Predictions based on these functions are also included in Fig. 13a. Both f_1 and f_2 give better predictions than f_{GS} and f_{QA} do, and as can be noted, f_2 fall right on top of the micromechanical results. A comparison was also made with results from a micromechanical analysis based on $m = 15$, and there, the prediction based on f_1, instead of f_2, was in closer agreement with the numerical results of the micromechanical model. This is attributed to differences in the plastic dissipation during crack advance through the synergistic effect where a change in lattice misorientation at a grain boundary is influenced by a change in plastic rate sensitivity, as discussed in relation to Fig. 11.

Predictions of the critical grain size as a function of the twist angle are compared with the micromechanical results in Fig. 13b. As noted, the trends predicted by g_{QA} and g_{GS} show no similarity at higher values of φ, where the QA-prediction falls significantly below the micromechanical results and the GS-prediction severely above the micromechanical results. At this juncture, it must be remembered that the topology of the cleavage planes in grain B are slightly different from the more physically correct topology on which the QA model is based (cf. Fig. 3a). In an attempt to rationalize the discrepancy between the QA-model and the micromechanical model, an angle function, $g(\varphi)$, was developed along the lines of the

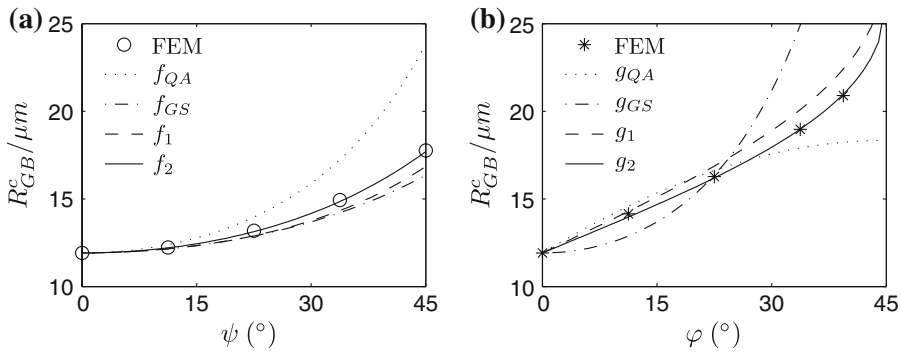

Fig. 13 Comparison between analytical expressions and numerical results for the influence of the misorientation on the critical grain size ($\Sigma_Z/\sigma_0 = 3.6$, $\Sigma_R/\Sigma_Z = 0.65$, $m = 25$). **a** Influence of tilt with $\varphi = 0°$. **b** Influence of twist with $\psi = 0°$

QA-model, accounting for the failing grain boundary area and primary/secondary cleavage planes in grain B, but tuned for the topology in the micromechanical model. However, that function did not result in a satisfactory prediction. A simple function, based on the relative area increase of secondary cleavage planes in grain B, turned out to work well. This function reads: $g_1 = 1 + (4h/w)/\cos(\varphi)$ (recall that for the current topology, $4h/w = (1 - \sqrt{\cos 2\varphi})/\tan\varphi$, see Sect. 2). The prediction based on g_1, also included in Fig. 13b, yields the same trend as the results from the micromechanical model, but slightly overestimates R^c_{GB}. A modification in the form of $g_2 = 1 + (\alpha \cdot 4h/w)/\cos(\varphi)$, with α fitted to 0.864, is in a very good conformity with the numerical results from the micromechanical model, as seen in Fig. 13b. For $m = 15$, the slightly lower value $\alpha = 0.715$ was obtained.

We close this Section by a comment on the generality of and the parameters that influence Eq. (11). Obviously, the critical grain size, $R^c_{GB}(0°, 0°)$, depends on many parameters as discussed in Sect. 4 and indicated by Eq. (9). It depends on temperature (through the rate exponent m) as seen in Fig. 11 and in Stec and Faleskog (2009) (see Figs. 12 and 13 in their paper), and on the properties of the grain boundary ($\Gamma^{GB} w / \left(\Gamma^B R_{GB}\right)$, β^{GB}) as seen in Fig. 9. Furthermore, if the temperature increases (increasing m) and/or the stress triaxiality decreases to a lower value than the one studied here ($\Sigma_R/\Sigma_Z = 0.65$), the active plastic dissipation during the dynamic crack propagation phase starts to increase from being fairly limited, cf. Stec and Faleskog (2009) (Figs. 17 through 19 in their paper). It is quite possible that the decoupled relation (11) may be valid also in such cases, but with functions $f(\psi)$ and $g(\varphi)$ that may not only depend on the misalignment angles.

6 Conclusions

In the present work, a microcrack that propagates dynamically over a grain boundary has been examined. Numerical findings based on the micromechanical model indicate the following:

1) When a microcrack enters a new grain, it does so first along the primary cleavage planes. During continued growth, the crack front is protruded along the primary cleavage planes and lags behind along the secondary cleavage planes.
2) The choice of cohesive parameters of the grain boundary has a large influence on the results, especially the parameter defining the shear strength of the cohesive zone.
3) In the presence of both tilt and twist misorientation, the critical grain size can accurately be expressed as $R^c_{GB}(\psi, \varphi) = R^c_{GB}(0°, 0°) \cdot f(\psi) \cdot g(\varphi)$ for the cases investigated here. The tilt influence can thus be separated from the twist influence, for which approximate expressions were proposed. The influence of the tilt angle, $f(\psi)$, can accurately be described by use of simple cosine functions, while the influence of the twist angle, $g(\varphi)$, is captured by the use of a function that describes the relative increase of the area of secondary cleavage planes.

Acknowledgments This investigation was initiated partly by funding from the Swedish Nuclear Power Inspectorate (SKI), now a part of the Swedish Radiation Safety Authority (SSM), which is acknowledged.

References

ABAQUS (2006) Standard-user's manual, version 6.6. Hibbit, Karlsson and Sorensen Inc., Providence, RI

Anderson T, Stienstra D, Dodds RH Jr (1994) A theoretical framework for addressing fracture in the ductile-brittle transition region. In: Landes JD, McCabe DE, Boulet JAM (eds) Fracture mechanics 24:th volume ASTM STP 1207. American Society for Testing of Materials, Philadelphia pp 186–214

Campbell JD, Ferguson WG (1970) The temperature and strain-rate dependence of the shear strength of mild steel. Philos Mag Lett 21:63–82

Clatterbuck DM, Chrzan DC, Morris JW Jr (2003) The ideal strength of iron in tension and shear. Acta Materialia 51:2271–2283

Crocker A, Smith G, Flewitt P, Moskovic R (1996) Grain boundary fracture in the cleavage regime of polycrystalline metals. In: Proceedings of the 11th European conference on fracture (EFC 11) Eng Mater Advis Serv, Warley, vol 1, pp 233–238

Faleskog J, Kroon M, Öberg H (2004) A probabilistic model for cleavage fracture with a length scale—parameter estimation and predictions of stationary crack experiments. Eng Fract Mech 71:57–79

Faleskog J, Stec M (2009) Micromechanics and probabilistic modeling of cleavage microcrack nucleation and growth caused by particle cracking. Report 466, KTH Engineering Sciences, Solid Mechanics, Royal Institute of Technology. Submitted for publication

Flewitt PEJ, Wild RK (2001) Grain boundaries. Their microstructure and chemistry. John Wiley & Sons, Ltd, Chichester

François D, Pineau A, Zaoui A (1998) Mechanical behavior of materials. Volume II: viscoplasticity, damage, fracture and contact mechanics. Kluwer Academic Publisher, Dordrecht

Gell M, Smith E (1967) The propagation of cracks through grain boundaries in polycrystalline 3% silicon-iron. Acta Metallurgica 15:253–258

Hamphreys FJ, Hatherly M (2004) Recrystallization and related annealing phenomena. 2nd edn. Elsevier Ltd, Oxford

Hahn GT (1984) The influence of microstructure on brittle fracture toughness. Metallurg Trans 15A:947–959

Klopp RW, Clifton RJ, Shawki TG (1985) Pressure-shear impact and the dynamic viscoplastic response of metals. Mech Mater 4:375–385

Kong X, Qiao Y (2005) Crack trapping effect of persistent grain boundary islands. Fatigue Fract Eng Mater Struct 28:753–758

Kroon M, Faleskog J (2005) Micromechanics of cleavage fracture initiation in ferritic steels by carbide cracking. J Mech Phys Solids 53:171–196

Kroon M, Faleskog J (2008) Influence of crack deflection into the carbide/ferrite interface on cleavage fracture initiation in ferritic steels. Mech Mater 40:695–707

Lee S, Kim S, Hwang B, Lee BS, Lee CG (2002) Effect of carbide distribution on the fracture toughness in the transition temperature region of an SA 508 steel. Acta Materialia 50:4755–4762

Linaza MA, Rodriguez Ibabe, Urcola JJ (1997) Determination of the energetic parameters controlling cleavage fracture initiation in steels. Fatigue Fract Eng Mater Struct 20:619–632

Martín-Meizoso A, Ocaña-Arizcorreta I, Gil-Sevillano J, Fuentes-Pérez M (1994) Modelling of cleavage fracture of bainitic steels. Acta Metallurgica et Materialia 42:2057–2068

McMahon CJ, Cohen M (1965) Initiation of cleavage in polycrystalline iron. Acta Metallurgica 13:591–604

Ortiz M, Pandolfi A (1999) Finite-deformation irreversible cohesive elements for three-dimensional crack-propagation analysis. Int J Numer Methods Eng 44:1267–1282

Qiao Y, Argon AS (2003a) Cleavage crack-growth-resistance of grain boundaries in polycrystalline Fe-2%Si alloy: experiments and modeling. Mech Mater 35:129–154

Qiao Y, Argon AS (2003b) Cleavage cracking resistance of high angle grain boundaries in Fe-3% Si alloy. Mech Mater 35:313–331

Qiao Y, Kong X (2004) An energy analysis of the grain boundary behavior in cleavage cracking in Fe-3wt.%Si alloy. Mater Lett 58:3156–3160

Roychowdhury S, Roy YDA, Dodds RHJr (2002) Ductile tearing in thin aluminum panels: experiments and analysis using large-displacement, 3-D surface cohesive elements. Eng Fract Mech 69:983–1002

Smith G, Crocker A, Flewitt P (2004) Brittle fracture of polycrystals: development of a new three-dimensional model. In: Proceedings of the 15th European conference on fracture (ECF15), CD-ROM, KTH, Stockholm

Stec M, Faleskog J (2009) Influence of grain size on arrest of a dynamically propagating cleavage crack in ferritic steels—micromechanics. Int J Fract 158:51–71

Tanguy B, Piques R, Laiarinandrasana L, Pineau A (1994) Mechanical behavior of a A508 steel based on a double nonlinear viscoplastic constitutive equation. In: Miannay D, Costa P, Francois D, Pineau A (eds) Euromat 2000, advances in mechanical behavior, plasticity and damage. Elsevier, Amsterdam pp 499–504

Wallin K (1991) Fracture toughness transition curve shape for ferritic structural steels. In: Teoh ST, Lee KH (eds) Fracture of engineering materials and structures. Elsevier Applied Science, Oxford pp 83–88

Wallin K, Laukkanen A (2006) Aspects of cleavage fracture initiation —relative influence of stress and strain. Fatigue & Fracture of Engineering Materials and Structures 29: 788–798